Available online at www.sciencedirect.com
SCIENCE DIRECT®
Journal of Power Sources 152 (2005) 131–145
JOURNAL OF POWER SOURCES
www.elsevier.com/locate/jpowsour

Water behavior in serpentine micro-channel for proton exchange membrane fuel cell cathode

Peng Quan [a], Biao Zhou [a,*], Andrzej Sobiesiak [a], Zhongsheng Liu [b]

[a] *Department of Mechanical, Automotive and Materials Engineering, University of Windsor, Windsor, Ont., Canada N9B 3P4*
[b] *Institute for Fuel Cell Innovation, National Research Council Canada, Vancouver, BC, Canada V6T 1W5*

Received 24 December 2004; accepted 15 February 2005
Available online 29 April 2005

Abstract

The behavior of water in the air–water flow inside a serpentine channel for a proton exchange membrane (PEM) fuel cell was investigated using the FLUENT software package. The volume-of-fluid (VOF) model was adopted to track the dynamic air–water interface. Five cases with varying initial water phase distribution corresponding to different fuel cell operating conditions were numerically simulated to obtain a better understanding of water behavior inside a serpentine micro-channel. Results show that the bend area of a serpentine flow channel has significant effects on the flow field, which in turn affects the air–water flow and water liquid distribution inside the channel or along the interior channel surfaces. The simulation results also indicate that water flooding could occur in the "after-bend" section of a micro-channel. For the case with larger amount of water in the two-phase flow, the simulation shows that the "after-bend" water distribution might block the reactant supply to reaction sites and, in some extreme situations, might block the reactant transport inside the flow channel, thus decreasing fuel cell performance.

Keywords: Proton exchange membrane fuel cells; Micro-channel; Water behavior; Two-phase flow; Volume-of-fluid

1. Introduction

Proton exchange membrane (PEM) fuel cell is the most promising power source for automotive and portable applications in the 21st century due to its high power density, relatively quick start-up, rapid response to varying loads, low operating temperature, and most importantly, zero emission, which is directly attributable to the reduction of air pollution and greenhouse effect. However, to achieve commercialization of fuel cells, the performance of contemporary PEM fuel cells needs to be significantly improved, by means of engineering optimization, to reduce the cost. As the core component of a PEM fuel cell, polymer membrane transferring protons across its thickness could only function well under fully saturated conditions due to the requirement of maintaining good proton conductivity [1]. Thus, water management has been a critical issue for fuel cell design and optimization and gained immense attention from both industry and academic institutions.

Water management should also be considered in porous electrodes and reactant flow channels. Since the operating temperature of a PEM fuel cell is lower than the boiling point of water, the inlet saturated gas stream could condense, consequently limiting mass transport by blocking reactant transport through the gas diffusion layer (GDL), especially at high current density. In addition, the non-uniform distribution of reactants over the effective electrode area, due to the non-uniformly distributed water pattern inside the gas flow channel, could result in poor cell performance. Thus, a better understanding of water behavior inside fuel cell components is highly desired for high-performance fuel cell design and optimization.

* Corresponding author. Tel.: +1 519 253 3000x2630; fax: +1 519 973 7007.
E-mail address: bzhou@uwindsor.ca (B. Zhou).

0378-7753/$ – see front matter © 2005 Elsevier B.V. All rights reserved.
doi:10.1016/j.jpowsour.2005.02.075

In the past decade, almost all the focus related to water management was on water retention and transport inside the membrane and gas diffusion layer. The model proposed by Springer et al. [2] considered both electro-osmotic drag and diffusion of water through the membrane. They concluded that water transported through the membrane could be insignificant compared to the amount of water generated from the electrochemical reaction in a PEM fuel cell. In 1993, Nguyen and White [3] presented a steady, two-dimensional heat and mass transfer model for a PEM fuel cell, which considered the transport of liquid water through the membrane by electro-osmotic drag and diffusion and included the phase-change of water. However, the membrane electrode assembly (MEA) was greatly simplified by assuming "ultra-thin" gas diffusion electrode. Bernardi and Verbrugge [4,5] and Springer et al. [2] investigated reactant transport through the GDL and only vapor-phase water transport was considered in the gas flow channel.

Water transport along the gas flow channel is very important for fuel cell design and optimization since this is where the product water leaves the cell. Water transport inside the gas flow channel is usually modeled as a component of an overall fuel cell model. The effect of water vapor on gas concentration along the reactant flow direction for various flow rates was simulated by Fuller and Newman [6] who showed that water and thermal management were tightly interrelated. In 1992, Kimble and Vanderborgh [7] proposed a model in which the effect of liquid water on the reactant concentration profile along the channel was considered. Yi and Nguyen [8] developed a multi-component, two-phase fuel cell model to evaluate the effects of various operating conditions on cell performance and concluded that counter-coolant flow was preferred for thermal and water management purposes. Recently, a hydraulic model along the flow direction using the Navier–Stokes equation was proposed by Gurau et al. [9]. They claimed that some of the convective flow along the gas flow channel could penetrate into the gas diffusion layer.

Some researchers have been trying to improve fuel cell performance by innovating gas flow channel configuration. An interdigitated channel design proposed by Amakawa and Uozumi [10] was greatly studied by other researchers [11–13]. This modified flow field configuration was expected to improve the reactant transport rate with a unique feature: driving liquid water out from the GDL to the gas flow channel. In 2001, a serpentine flow field design was reported to improve the utilization of the electrode area under the rib [14]. The corresponding modeling work, which considered both a straight flow field and a serpentine flow field with pressure variation along the flow channel, was presented by Dutta et al. [14,15]. However, effects of the bends in the gas flow channel on the flow dynamics were not included.

To date, most of the flow field models have focused on flow field plates with simple structures, such as conventional straight flow and grid flow channels and thus a model for the commonly used serpentine flow field is highly desired. In addition, the two-phase flow characteristics in a gas flow micro-channel are significantly different from those of larger channels, with respect to two-phase pressure drop [16,17] and two-phase flow pattern [16,18]. In the present work, an attempt, at seeking a practical approach that is capable of simulating the fluid dynamics and predicting liquid water distribution in a serpentine micro-channel without involving details of electrochemical reaction, was made. It is well known that the electrochemical reaction is the key for a high-performance fuel cell. However, considering the fact that no electrochemical reaction is involved inside the gas flow channel and the water inside the micro-channel comes from either the electrode surface (liquid water produced through electrochemical reaction in the catalyst layer is transported through the porous electrode and enters the gas flow channel) or being carried in by feeding reactant, the current problem could be simplified as a fluid mechanics problem with water sources inside its physical domain or on its boundaries.

In the following section, the numerical model, boundary conditions, as well as the grid independency validation are introduced. The main body of the work, the 3D numerical simulation of water behavior in part of the serpentine micro-channel for a PEM fuel cell cathode performed by use of a commercial computational fluid dynamics (CFD) software, the FLUENT package [19], is presented in the third section. Five cases with varying initial water phase distribution were simulated to investigate the two-phase flow inside a gas flow channel under five possible and typical fuel cell operating conditions. Finally, in Section 4, conclusions from the numerical study are drawn.

2. Numerical model and boundary conditions

2.1. Physical and computation domain

A U-shaped micro-channel is the key component of a serpentine gas flow channel, which is extensively used in PEM fuel cells. Fig. 1 shows a schematic illustration of the computation domain employed showing the U-shaped channel of 40 mm long for a round-trip with rectangular cross-section of 1 mm × 1 mm. The simulations using one

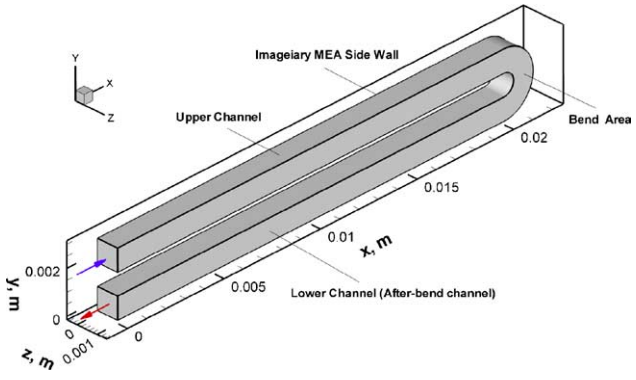

Fig. 1. Part of the serpentine cathode channel for the numerical simulation.

U-shaped micro-channel are capable of providing invaluable information for fuel cell flow field design and optimization.

2.2. Boundary conditions

The air–water transport process inside the micro-channel is modeled as a 3D transient two-phase flow. No-slip boundary condition is applied to all interior walls. A velocity inlet boundary condition (uniform velocity distribution of $10\,\mathrm{m\,s^{-1}}$ with direction normal to the inlet boundary) was applied at the inlet of the channel. At the outlet, the boundary condition was assigned as outlet flow (the gradients of all flow parameters are zero). To simulate water behavior under various PEM fuel cell operating conditions, initial water distribution inside the computation domain was carefully set up and the details are given in Section 3.

2.3. Computational methodology

The numerical simulation for a 3D transient two-phase flow in the U-shaped micro-channel was performed using the FLUENT software. An inspection of the numerical setup employed showed that the Reynolds number of the flow inside the channel was less than 700 hence indicating that the flow was in the laminar regime. It was also assumed that the flow was under isothermal conditions, i.e., the flow was considered without temperature variation. The conservation equations governing an unsteady laminar flow can be written as [19]:

- Continuity equation:

$$\frac{\partial \rho}{\partial t} + \nabla \cdot (\rho \vec{v}) = 0 \tag{1}$$

- Momentum equation:

$$\frac{\partial (\rho \vec{v})}{\partial t} + \nabla \cdot (\rho \vec{v} \vec{v}) = -\nabla p + \nabla \cdot (\bar{\bar{\tau}}) + \rho \vec{g} + \vec{F} \tag{2}$$

where p is the static pressure, $\vec{F}$ a momentum source term due to surface tension, and $\bar{\bar{\tau}}$ the stress tensor, which is given by

$$\bar{\bar{\tau}} = \mu(\nabla \vec{v} + \nabla \vec{v}^{\mathrm{T}}) - \tfrac{2}{3}\mu \nabla \cdot \vec{v} I \tag{3}$$

where μ is the dynamic viscosity and I the unit tensor.

To track the air–water interface inside the computation domain, the volume-of-fluid (VOF) model implemented in the FLUENT [19] was adopted. The VOF model was designed for two or more immiscible fluids, where the position of the interfaces between fluids is of interest. In the VOF model, an advective equation for volume fraction, F, needs to be solved and the reconstruction of the interface throughout the computation domain is required. For the ith phase, the volume fraction equation has the following form:

$$\frac{\partial F_i}{\partial t} + \vec{v} \cdot \nabla (F_i) = 0 \tag{4}$$

The volume fraction for the primary phase (air in the present study) can be computed based on the following constraint:

$$\sum_{i=1}^{n} F_i = 1 \tag{5}$$

For a multi-phase mixture, the average properties could be obtained through interpolation, for instance, the mixture density ρ can be calculated as:

$$\rho = \sum F_i \rho_i \tag{6}$$

The effects of surface tension along the interface between each pair of phases and wall adhesion play an important role in the two-phase flow process in the micro-channel and it could be included in the VOF model [19]. In the present work, a widely used surface tension model, the continuum surface force (CSF) model proposed by Brackbill et al. [20] was adopted. With this model, the consideration of surface tension results in a source term, $\vec{F}$ in the momentum equation (2). Additionally, effects of wall adhesion were taken into account by specifying a wall adhesion angle in conjunction with the CSF model in the FLUENT throughout the simulation.

2.4. Validation of grid independency

In the present study, a 3D structured orthogonal grid with about 358,000 computation nodes was employed. The grid independency was validated by performing numerical simulation for one droplet case (Case 1 in Table 1) with varying number of nodes. This original grid has been refined twice by adding 20 and 40% of the cell number in every direction leading to a 95.0 and 204.5% finer grid, respectively. Simulation results showed that it was almost impossible to distinguish the droplet outlines among these three different-node-number cases at the same time instant. In addition, because computational cost (iteration per second) increased linearly with increasing number of nodes, considering the processing time limitation, the original computational grid with 358,000 nodes was adopted for all simulation cases presented in this study.

3. Results and discussions

To investigate water behavior in the two-phase flow along a serpentine micro-channel for a PEM fuel cell, five numerical setups in the order of increasing initial water content were designed to simulate corresponding possible and typical fuel cell operating conditions as listed in Table 1. The issues, which are of importance to fuel cell flow channel design and optimization, are addressed in the following related sections.

Table 1
Five simulation cases for varying PEM fuel cell operating conditions

Case no.	Inlet velocity ($m\,s^{-1}$)	Initial water (mm^3)	Initial water distribution	Corresponding PEM fuel cell operating condition
1	10	3.35×10^{-2}	Single spherical droplet ($r = 0.2$ mm) freely suspended at micro-channel inlet	Fundamental study of droplet deformation inside the airflow micro-channel
2	10	1.81	A series of droplets ($r = 0.2$ mm) freely suspended along a micro-channel centerline	Feeding reactant flow with liquid water for saturation
3	10	1.53	A series of droplets ($r = 0.2$ mm) attached to a side wall of micro-channel (distance between droplet center and wall is 0.1 mm)	Small amount of liquid water generated or condensed on the surface of MEA sidewall
4	10	9.20	A liquid water film with thickness of 0.2 mm covering the imaginary MEA surface	Large amount of liquid water generated or condensed on the surface of MEA side wall
5	10	16.10	A liquid water film with thickness of 0.1 mm covering all interior surfaces of the micro-channel	Extreme case—large amount of liquid water, due to electrochemical reaction, water condensation or reactant feeding, covering all interior surfaces

3.1. Case 1: a single droplet freely suspended at the entrance of micro-channel

In Case 1, a single droplet with diameter of 0.2 mm was initially placed at the inlet of the micro-channel. The simulation for the single droplet case was performed to investigate droplet deformation and the interaction between the droplet(s) and the surrounding airflow in both the straight and bend sections.

3.1.1. Single droplet deformation and behavior in bend area

Fig. 2 shows the droplet deformation versus time on the center-plane of z-direction when a droplet travels in the U-shaped channel. At $t = 0$, the droplet was placed at the channel inlet and was in its initial spherical shape. As time progressed, droplet deformation (elongation) in the flow direction, which is due to a combination of droplet surface tension and shear stress from surrounding airflow, could be observed. In other words, the enlargement of droplet surface area increased the surface tension such that the force balance on the droplet could be achieved. With further development, smaller droplets would form and be separated from the original droplet, as shown in the close-to-the-bend area ($t = 1.25$, 1.4, 1.6 and 1.85 ms) in Fig. 2. This indicates that the surface tension is not sufficient to prevent disintegration of the original droplet.

Furthermore, Fig. 2 also shows that there was only a slight displacement in the vertical (y coordinate) direction when water droplet(s) traveled in the straight channel. Therefore, it could be concluded that the effect of gravity is not significant compared to that of inertia force for this small-amount-of-water micro-channel application.

3.1.2. Air–water behavior in bend area

With the deformed droplets approaching the U-shaped bend, the velocity field in the vicinity of the outer bend surface varied dramatically. The originally slightly branched velocity field expanded significantly due to the fact that the approaching droplets squeezed the airflow between the droplets and bend-wall surface to the surrounding space; clearly demonstrated in Fig. 3.

When the deformed droplets hit the bend-wall surface, one or more higher-pressure zones could be observed near the bend surface as shown in Fig. 4. The formation of these high-pressure zones is due to the collision (momentum exchange) of the droplets against the bend-wall surface. It is the collision that significantly affected the water behavior since both the velocity field and the water droplet distribution changed significantly compared to those before the collision.

Driven by the expanding airflow, the deformed droplets moved to the corner areas (or the intersections of side walls and outer bend surface) and then moved downstream along

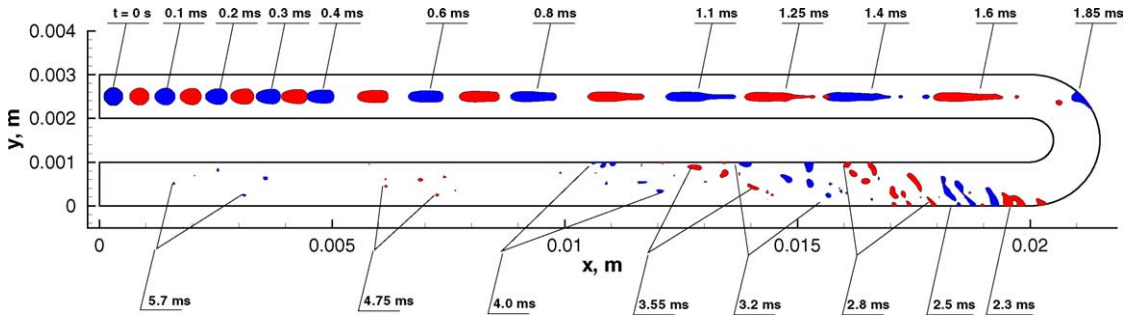

Fig. 2. The deformation of a single droplet at different time instants inside U-shaped micro-channel.

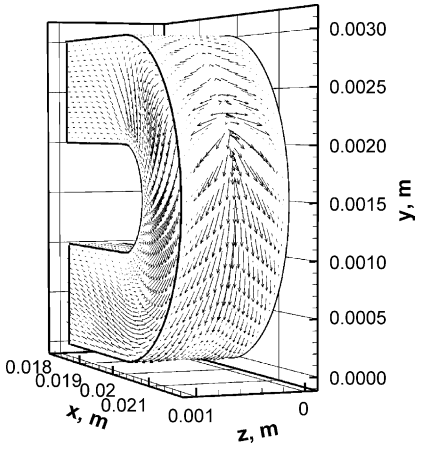

Fig. 3. Velocity field on the surface near the outer bend surface before droplets reach the bend wall (t = 1.75 ms).

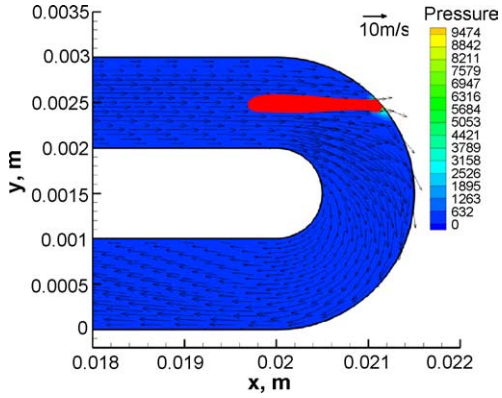

Fig. 4. Water liquid, velocity distribution and gauge pressure (Pa) on the center-plane of z-direction at t = 1.85 ms.

the corner edges as shown in Fig. 5a and b. This could be explained by the fact that the wall adhesion effect in the corner area is more significant compared to that in the center of the bend surface since the corner region doubles the contact area between the walls and water.

It is also noteworthy that small droplets might form when the deformed water droplets traveled down along the bend surface, since the velocity difference between airflow in the channel center and that in the vicinity of corners could provide strong shear stress resulting in fragmentation of a bigger droplet into smaller ones as shown in Fig. 5b.

3.2. Case 2: a series of droplets freely suspended along the centerline of the U-shaped micro-channel

In the second case, a series of spherical droplets with diameter of 0.2 mm were freely suspended along the centerline of the U-shaped micro-channel. By increasing the number of water droplets, this case could be considered as an extension of Case 1 and used to simulate the fuel cell operating condition with some water carried in by feeding reactant. In addition, the interaction between droplets could be taken into account for this multi-droplet case.

3.2.1. Droplet deformation

Contrary to Case 1, an individual droplet in the second case experienced a different deformation process. With time progressed, the windward surface of the originally spherical droplets gradually flattened, while the leeward surface did not elongate due to constraints from its neighboring droplet, subsequently forming a parachute-shaped droplet. The authors believe this kind of droplet deformation could be caused by the non-uniform velocity distribution around the droplet. Fig. 6 clearly shows the velocity difference between the windward and leeward region for several droplets around the bend area.

Fig. 6 also indicates that, after hitting the bend surface, these deformed droplets had the tendency of fragmenting and then entering the central airflow due to the dragging effect from the “U-turn” flow (inside the bend of a U-shaped micro-channel, a flow that must make a U-turn due to constraints from the bend was termed “U-turn” flow throughout this work). Obviously, in the bend area, the shear force

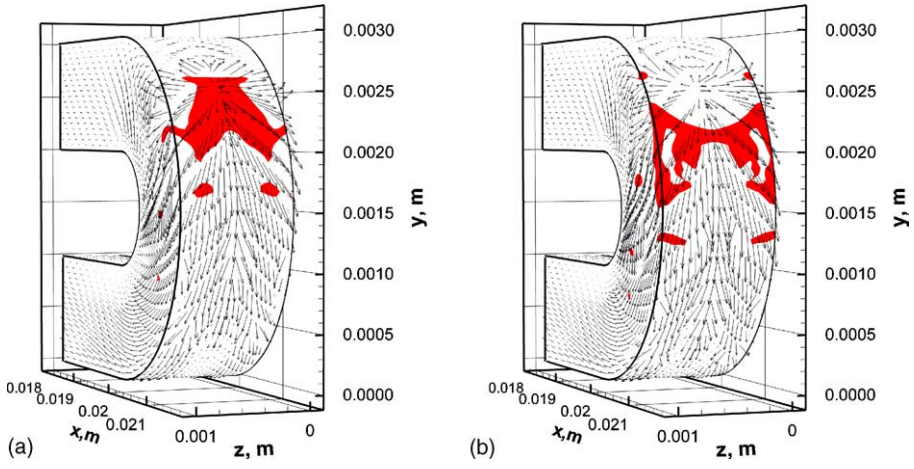

Fig. 5. Development of water pattern and velocity field on the surface near the outer bend surface: (a) t = 1.95 ms; (b) t = 2.00 ms.

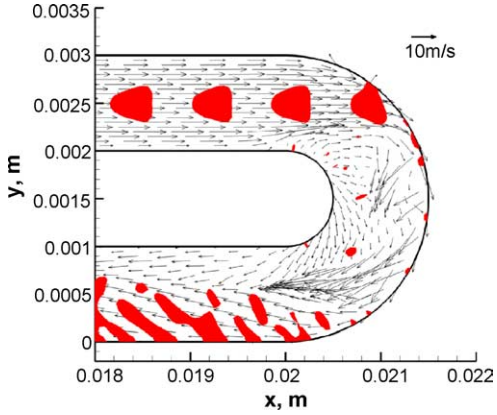

Fig. 6. Velocity distribution around droplets on the center-plane of z-direction in the bend area at $t = 1.70$ ms.

from the airflow is much stronger than the droplet surface tension, thus together with the inertia force, resulting in significant droplet deformation and dramatic water liquid distribution.

3.2.2. *Water behavior in the bend area*

As earlier mentioned, droplets in the upper straight channel experienced a "parachute" deformation. However, for the initially placed four droplets inside the bend area, as shown in Fig. 7a, significant elongation could be observed at the beginning ($t = 0.1$ ms). This deformation was caused by the shear stress from the "U-turn" airflow in the bend area.

At $t = 0.3$ ms, the four deformed droplets were further elongated and the strong "U-turn" airflow cut these deformed droplets into even smaller ones which could move with the airflow or hit the bend surface as shown in Fig. 7b.

At $t = 0.4$ ms, the droplet that first entered the bend from the upper straight channel hit the bend-wall surface. This droplet and previously formed smaller ones could induce a series of high-pressure zones near the outer surface of the bend, as shown in Fig. 7c. The variation of corresponding velocity field, which is the driving force to move the water downstream, is shown in Fig. 8a–c. The overall trend of water movement on the surface adjacent to the outer bend surface: bigger droplets hit the bend wall and expanded to the surroundings of the landing point then moved downstream, is also illustrated in the same set of figures.

After 1 ms, the overall water pattern on and adjacent to the bend wall became stable. Fig. 8c shows a typical "band" pattern on the surface near the outer surface of the bend wall at $t = 1.3$ ms. Driven by the shear force from the surrounding expanding airflow, these "water bands" moved downwards along the bend surface, meanwhile, to the corners formed by the outer bend surface and side walls. It can be observed that, during the process, the "water bands" might be torn into smaller pieces by the expanding airflow due to the non-uniformly distributed velocity field.

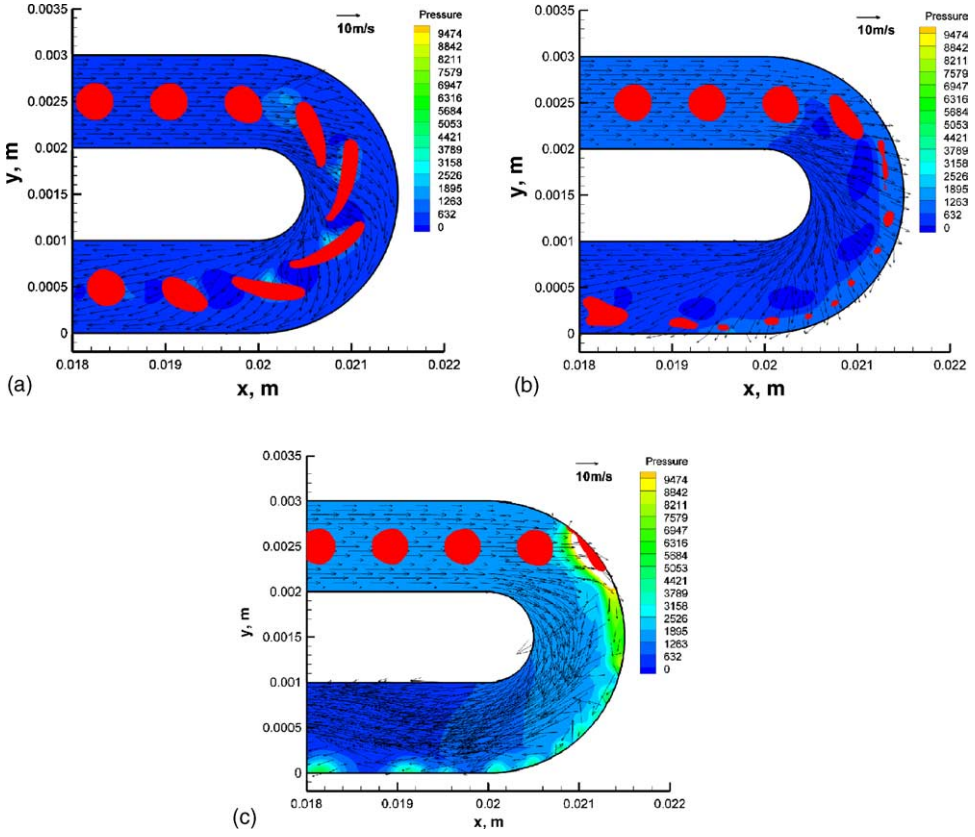

Fig. 7. Water liquid, velocity field and gauge pressure (Pa) on the center-plane of z-direction: (a) $t = 0.1$ ms; (b) $t = 0.3$ ms; (c) $t = 0.4$ ms.

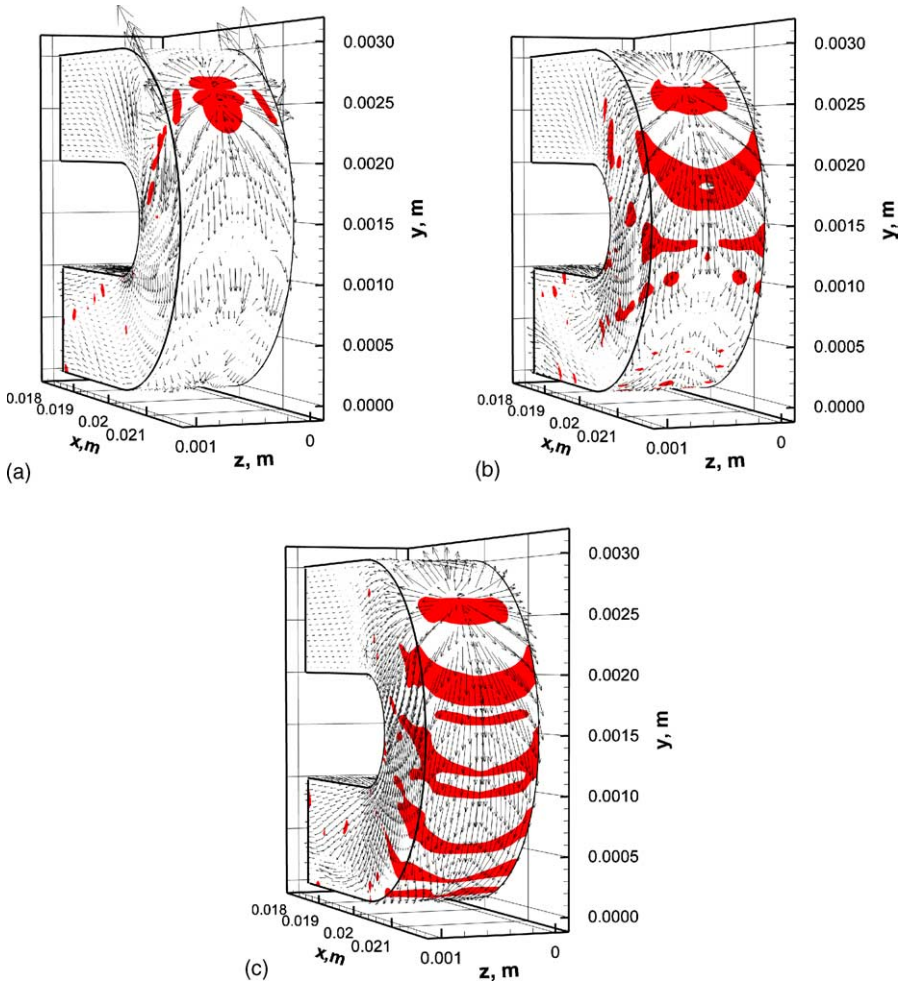

Fig. 8. Water liquid and velocity distribution on the surface near the outer bend surface: (a) $t = 0.4$ ms; (b) $t = 0.6$ ms; (c) $t = 1.3$ ms.

3.2.3. *Secondary flow development in bend area*

A significant secondary flow, two axisymmetric vortices occupying the whole channel cross-section, could be observed in the bend area. To investigate the evolution of the secondary flow along the main flow direction and the interaction between the secondary flow and the water liquid in the bend area, several cross-sections were extracted as shown in Fig. 9 for a typical instant at $t = 3$ ms when a fully developed "band" pattern shown on the surface close to the outer bend surface.

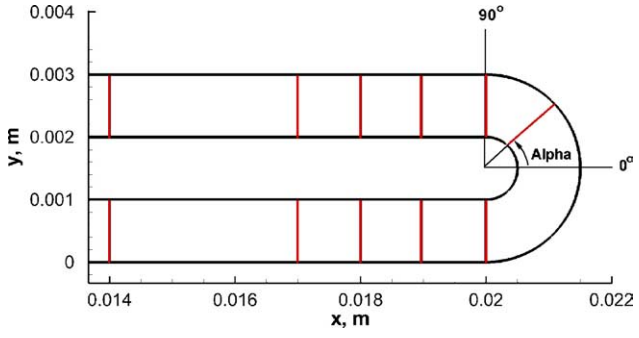

Fig. 9. Diagram for the selected cross-sections along the main flow direction.

Fig. 10 shows the variation of secondary flow in different cross-sections at varying angles defined in Fig. 9. For the flow before the bend, there were not significant vortices as shown in Fig. 10a. At the bend inlet (Fig. 10b, i.e., $\alpha = 90^\circ$), the two axisymmetric vortices appeared in the cross-section. The velocity magnitude in the surroundings of the vortices was much greater than that in the center. From the cross-section $\alpha = 30^\circ$ (Fig. 10c) through $\alpha = -30^\circ$ (Fig. 10e), the two vortices were further reinforced, particularly in the center of the cross-section, which could enhance the water movement to wall surfaces. Meanwhile the number of vortex was increasing, and thus a multi-vortex structure gradually developed. The multi-vortex structure could significantly enhance air–water mixing and make water liquid more evenly distributed in the airflow inside the micro-channel. After $\alpha = -60^\circ$ (Fig. 10f), this structure became weak, especially in the straight after-bend channel, for instance, at $x = 0.012$ m (Fig. 10h), the flow maintained the multi-vortex structure, but it was very weak.

From the above analysis, the authors concluded that the impact of bend on the air–water flow was very important, because there were no any other driving forces provided to the flow except for the ones due to the bend area. In other words,

it was the presence of the bend that changed the air–water flow field and water liquid distribution along the main flow direction, which could have significant impacts on reactant diffusion to the reaction sites and water transport inside the micro-channel.

3.2.4. Water behavior in the after-bend area

Passing through the bend area, the water liquid would move downstream to the after-bend channel. Fig. 11 shows the water pattern development on the center-plane of z-direction inside the gas flow micro-channel. In Fig. 11a, the deformation of the last droplet (in flow direction) in the lower straight after-bend channel, due to the up-bend airflow at the bend exit is clearly shown. The up-bend airflow, caused by the interaction between water liquid attaching to the lower outer bend surface and the "U-turn" airflow adjacent to it, could be observed at the position of around $x = 0.02$ m in the lower channel. By providing a strong dragging force, this

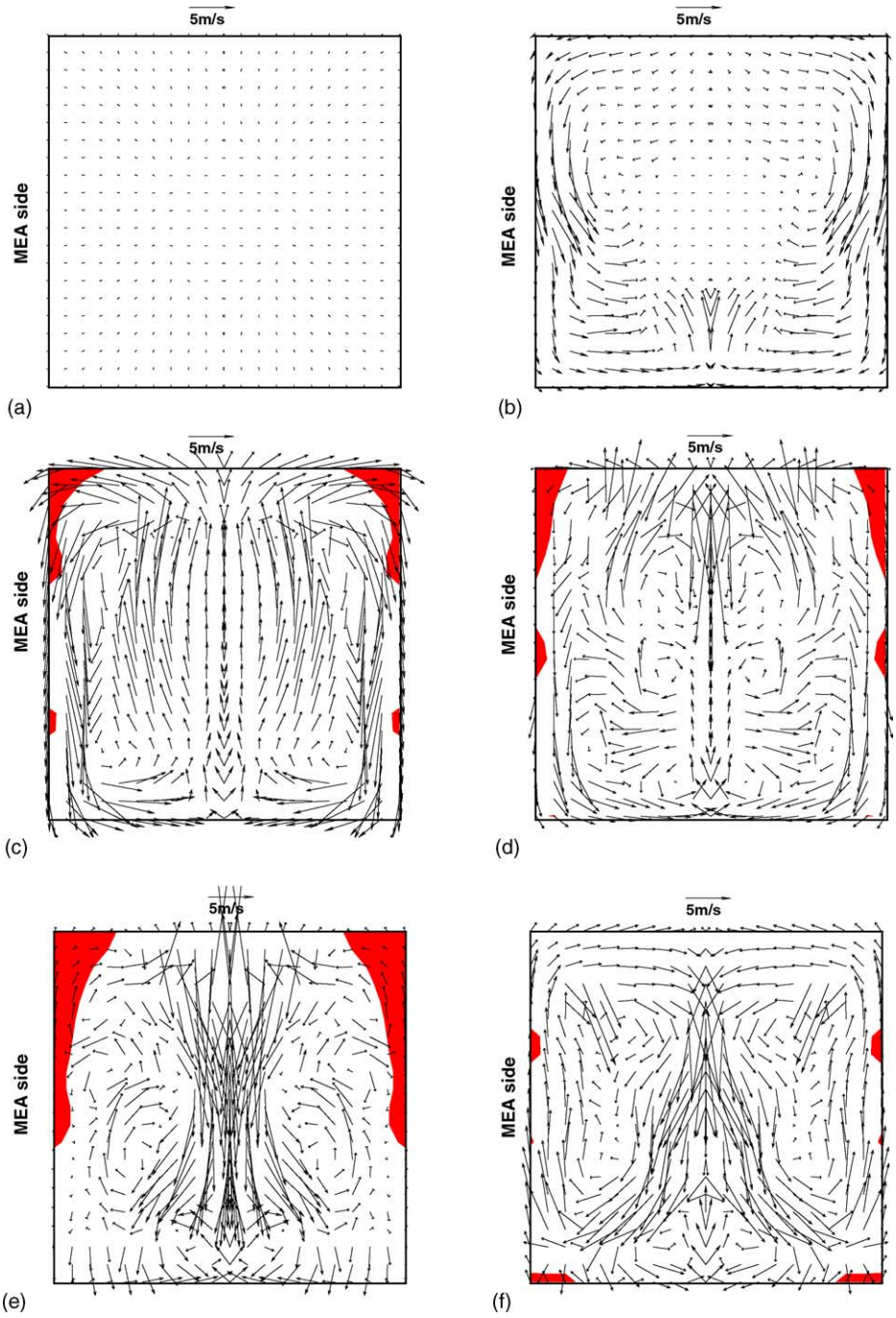

Fig. 10. Water liquid distribution and velocity distribution in different cross-sections in bend area at $t = 3$ ms: (a) $x = 0.018$ m in upper channel; (b) $\alpha = 90°$; (c) $\alpha = 30°$; (d) $\alpha = 0°$; (e) $\alpha = -30°$; (f) $\alpha = -60°$; (g) $\alpha = -90°$; (h) $x = 0.012$ m in lower channel.

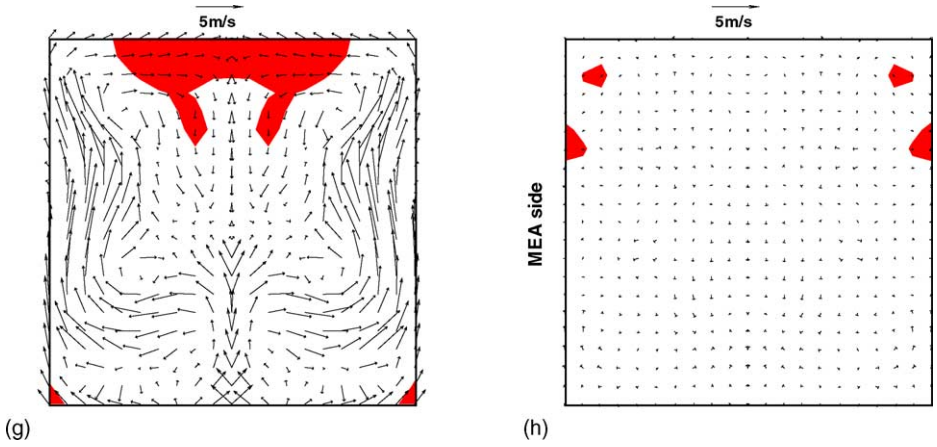

Fig. 10. (*Continued*).

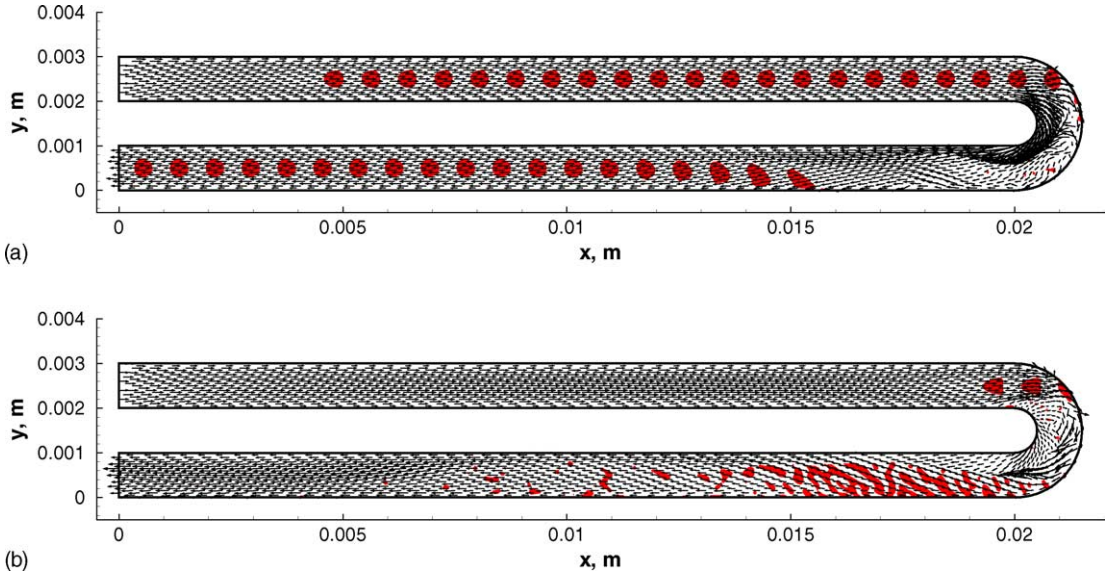

Fig. 11. Water behavior in the center-plane of z-direction at different time instants: (a) $t = 0.5$ ms; (b) $t = 1.8$ ms.

up-bend airflow could move the liquid water attaching on the outer surface towards inner surface of the after-bend channel, as shown in Fig. 11b. This process might also enhance the fragmentation of bigger droplets, thus making the liquid water more evenly distributed within the after-bend straight channel, which could be beneficial to maintain the airflow near full saturation. A typical water distribution ($t = 2.3$ ms) in cross-sections along the main flow direction is shown in Fig. 12.

3.3. Case 3: a series of droplets attached to the imaginary MEA side wall of the micro-channel

Following the second case, this time the authors attached all the previously suspended droplets to a side wall (the distance between the center of droplets and wall was 0.1 mm), which could be imagined as the porous electrode surface of a PEM fuel cell with liquid water generated from or condensed on it.

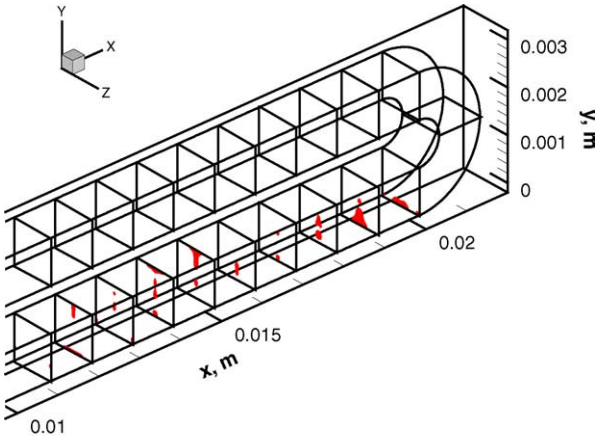

Fig. 12. Water distribution in the cross-sections along the flow direction at $t = 2.3$ ms.

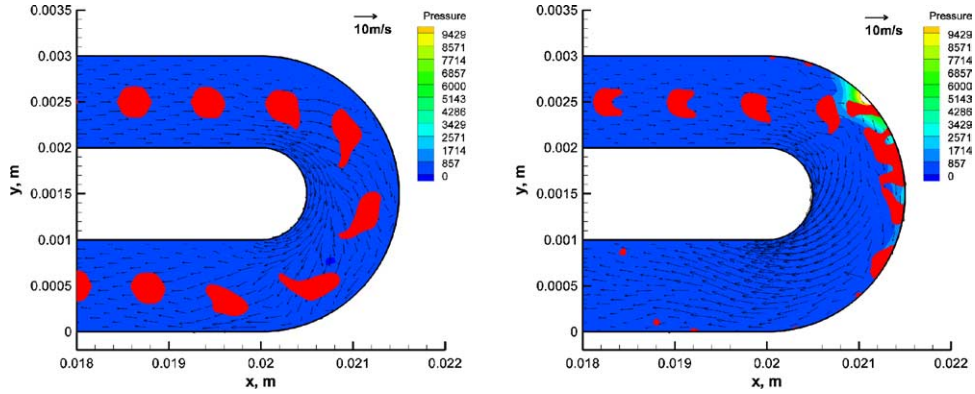

Fig. 13. Water liquid, velocity distribution and gauge pressure (Pa) on the plane near the imaginary MEA sidewall: (a) $t = 0.3$ ms; (b) $t = 0.75$ ms.

3.3.1. Water behavior in bend area

For Case 3 with droplets attached to the side wall, wall adhesion affected the water behavior significantly throughout the simulation. Thus, as expected, the motion of droplets was delayed comparing to Case 2. This is clearly demonstrated in Fig. 13a and Fig. 7b, which show the water pattern and velocity/pressure distribution for Case 3 in a plane very close to the imaginary MEA sidewall and for Case 2 on the center-plane of z-direction at the same instant ($t = 0.3$ ms), respectively. In addition, as shown in Fig. 13b, the deformation of a single droplet in the upper straight channel became more parachute-like due to significant wall adhesion.

In the bend area, the water behavior was in a similar manner as in Case 2, except that for Case 3, the "water bands" appeared at the location close to the MEA side. Fig. 14a shows a typical offset "band" pattern on the surface close to the outer bend surface at $t = 2.15$ ms. Similar to the phenomena observed in Case 2, a high-pressure zone at the water–wall contact region could also be observed at the same instant, as shown in Fig. 14b.

It should be noted that, from Fig. 14b, a significant circulating flow along the upper edge formed by imaginary MEA sidewall and outer bend surface could be observed. The authors believe that this is evidence that, in the edge area, the velocity is relatively small due to constraints from wall boundaries. Obviously, this circulating zone may hold some of the water transferred from reaction sites or upstream flow and reduce the effective electrode area through which the reactant could diffuse to the reaction sites.

3.3.2. Secondary flow development

To investigate the variation of secondary flow in the bend area, some cross-sections (as shown in Fig. 9) were extracted along the main flow direction at $t = 3.95$ ms when flow pattern became "pseudo-steady" (sufficient water droplets were provided from the upper straight channel to the bend, thus resulting in the steady-like water pattern on the surface near the outer bend surface). The velocity/water distribution in these cross-sections is shown in Fig. 15a–h.

In the upper channel before the bend, the vortex effect was not significant as shown in Fig. 15a. However, inside

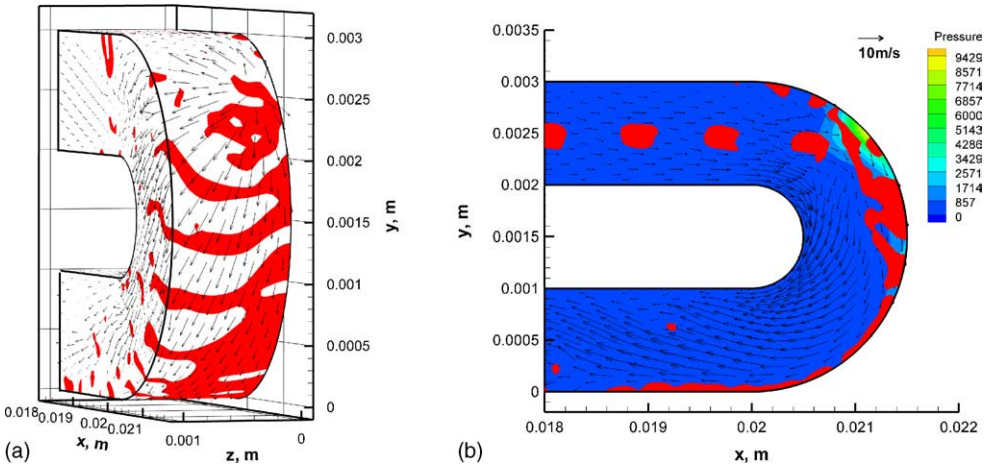

Fig. 14. (a) Water liquid and velocity distribution on the surface near the outer bend surface at $t = 2.15$ ms. (b) Water liquid, velocity distribution and gauge pressure (Pa) on the plane near the imaginary MEA sidewall at $t = 2.15$ ms.

the bend, a double-vortex structure could be observed at the beginning of the bend, for instance, in the cross-section of $\alpha = 75^\circ$, although the axisymmetry became weak due to the droplets attached to the imaginary MEA side wall (the droplets could not be observed in this cross-section). From $\alpha = 45^\circ$ (Fig. 15d) through $\alpha = -45^\circ$ (Fig. 15f), the original two vortices were fragmented into several smaller ones which occupied the whole channel cross-section and thus could enhance the air–water mixing in the bend. The formation of this multi-vortex structure was caused by the interaction of the airflow and the non-uniformly distributed water liquid on the interior surfaces of the bend. When the air–water flow approached the lower straight channel, these smaller vortices were seen to fade away. A single full-scale vortex gradually developed as shown in Fig. 15g and h. Although the intensity of the full-scale vortex was not as strong as that in the bend, it could provide a force to keep the on-the-wall water remaining on the interior surfaces of the channel, and in some way, deliver small dispersed droplets to the surrounding interior surfaces, thus affecting the reactant diffusion to reaction sites.

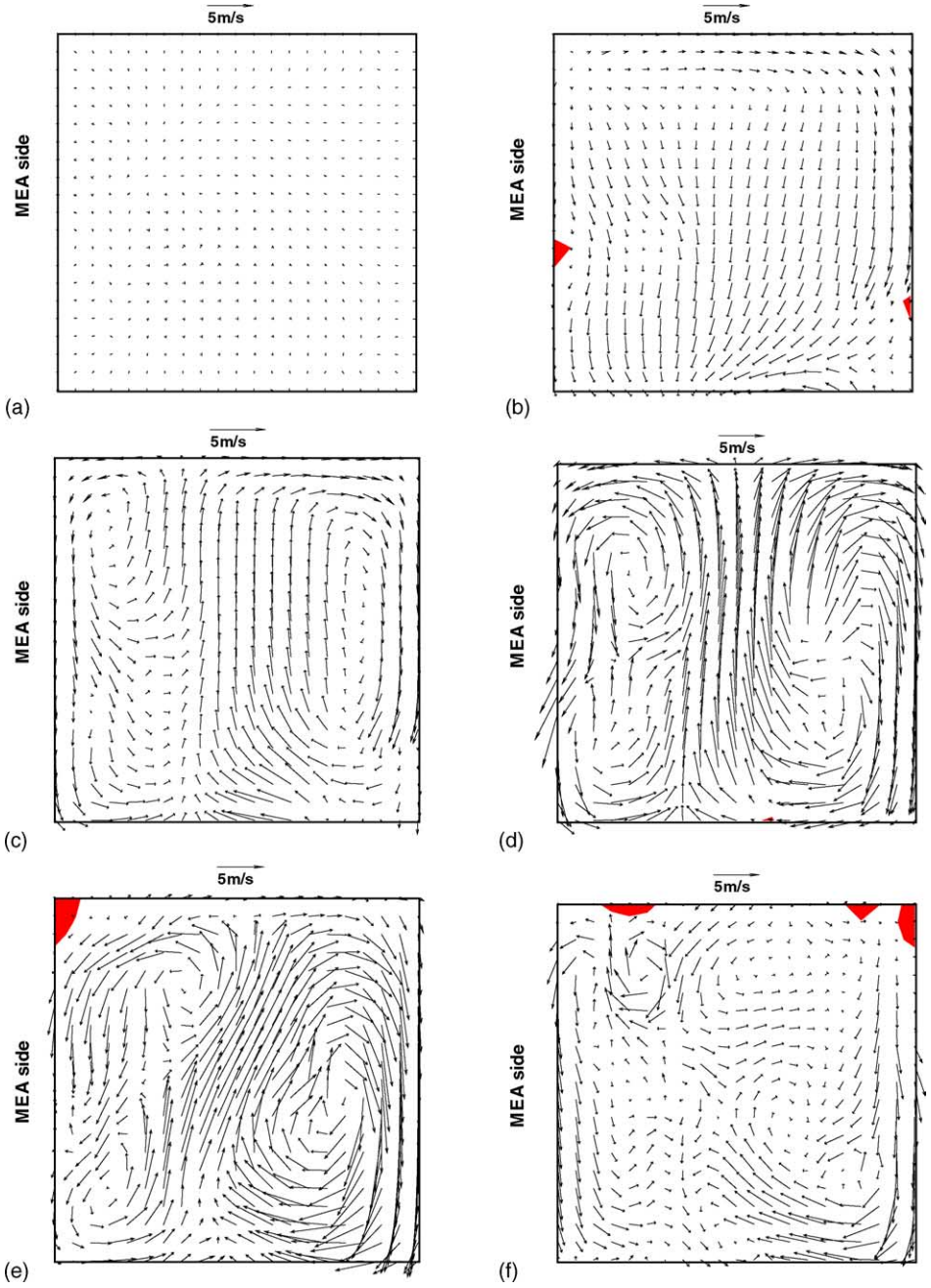

Fig. 15. Water and velocity distribution in different cross-sections along the main flow direction at $t = 3.95$ ms: (a) $x = 0.017$ m in upper channel; (b) $\alpha = 90^\circ$; (c) $\alpha = 75^\circ$; (d) $\alpha = 45^\circ$; (e) $\alpha = 0^\circ$; (f) $\alpha = -45^\circ$; (g) $\alpha = -90^\circ$; (h) $x = 0.017$ m in lower channel.

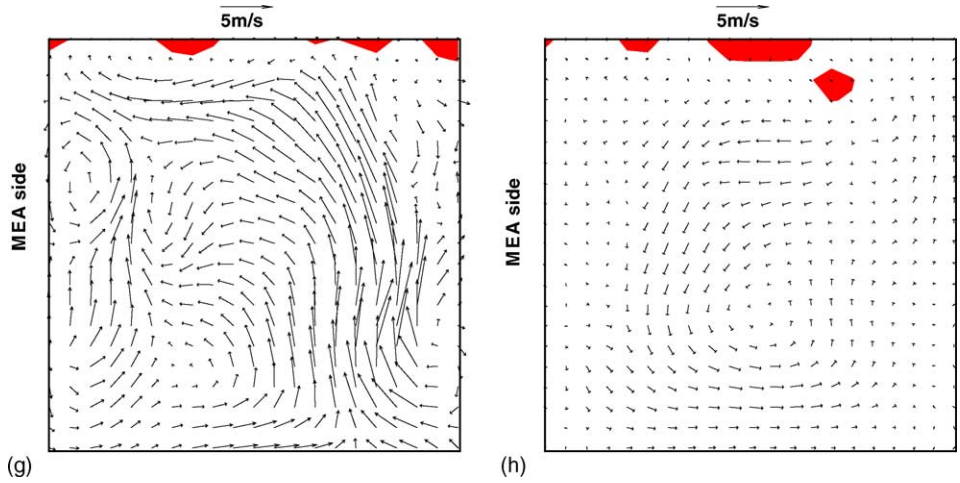

Fig. 15. (*Continued*).

3.4. Case 4: a liquid water film covering the imaginary MEA sidewall of a micro-channel

In the fourth case, a layer of liquid water with thickness of 0.2 mm was initially attached to the imaginary MEA sidewall to simulate the working condition with more water generated from the electrochemical reaction. Wall adhesion played an important role in this simulation; particularly, the combination of wall adhesion, water surface tension, and the shear force from airflow had significant impacts on the water behavior in the bend area.

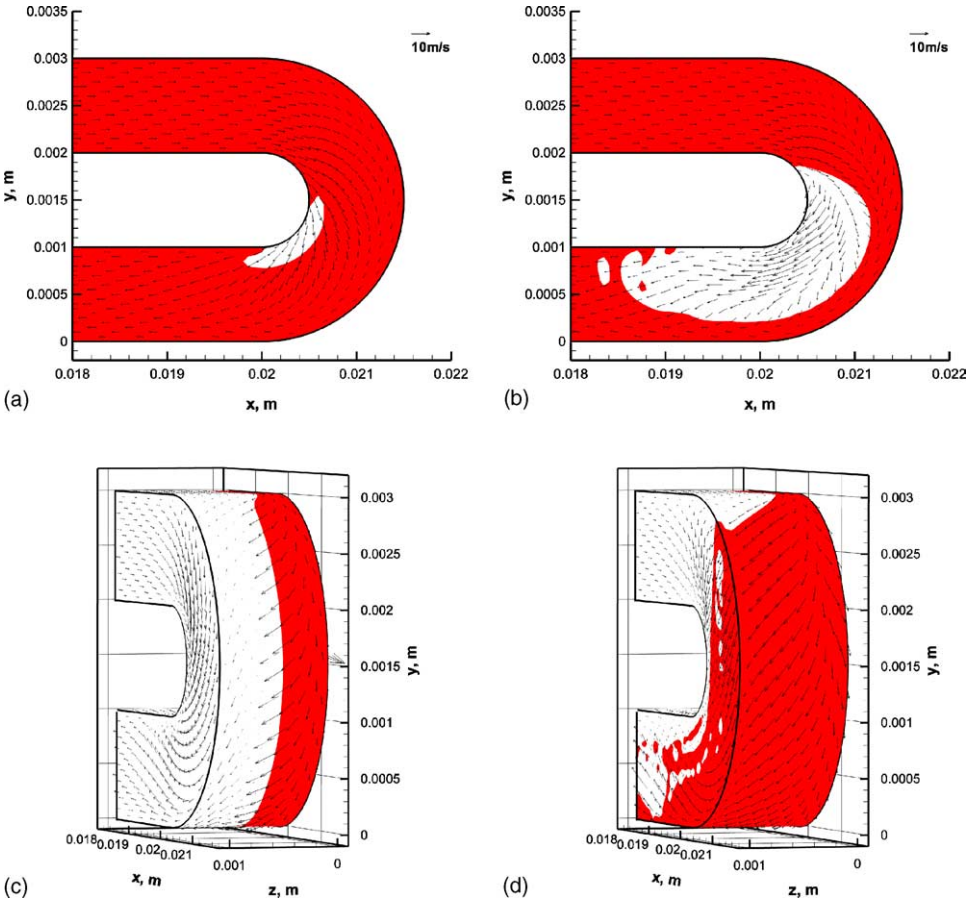

Fig. 16. Water liquid and velocity distribution on the plane near the imaginary MEA sidewall: (a) $t = 0.25$ ms; (b) $t = 0.45$ ms; and on the surface near the outer bend surface: (c) $t = 0.25$ ms; (d) $t = 0.45$ ms.

3.4.1. The formation of void space on the plane close to the imaginary MEA side wall in the bend area

In the bend area, the layer of liquid water experienced similar process to that of Case 3. However, due to considerable increase in the amount of water, some unique water behaviors, which are directly related to the water and reactant transport in the micro-channel, could be observed.

Figs. 16 and 17 illustrate the formation of a void space on the plane close to the imaginary MEA sidewall in the bend area. At $t = 0.25$ ms (Fig. 16a), a small void space formed on the initially uniform water film and then continued to grow up due to the effect of inertia force as shown in Fig. 16b. Driven by the shear force from the surrounding airflow, the water film on the imaginary MEA side surface inside the lower channel continuously moved downstream to the exit of the lower channel, thus developing more void space as shown in Figs. 16b and 17a. Meanwhile, with more water moving from the upper straight channel to the bend, the moving water film reached the bend surface and started to expand and cover the entire bend surface, which could be observed in Fig. 16c and d.

Due to the interaction between water liquid and airflow, the "U-turn" airflow would be bent up after leaving the bend exit in the lower channel. Fig. 17b and c shows that the up-bend airflow would continuously drag the liquid water from the bottom surface to the sidewalls and upper surface of the micro-channel. The developing velocity field also provided a thrust to the newly formed water front and moved it to the exit of the lower channel, thus making more void space; this is clearly shown in Fig. 17c and d.

Although liquid water would be continuously generated from the cathode surface under the working condition of a real fuel cell, the constantly developing void space can be capable of making more effective electrode surface area exposed to reactant flow and maintaining the effective mass transport inside the micro-channel.

For Case 4, the variation of secondary flow along flow direction in the bend was quite similar to that observed in Case 3. Fig. 18 shows the water liquid distribution in the cross-sections along the flow channel at 3.75 ms. In the cross-sections close to the bend, the void space effect and relatively weak vortices made the water liquid move along the bottom surface of the lower channel and then the water could be moved up to the side walls and upper surface by the up-bend airflow as previously observed. In the lower straight channel, the water distribution in the cross-sections would be strongly affected by the full-scale vortex, which could bring water liquid to the surrounding walls, eventually blocking the path that the reactant is transported to the reaction sites through the imaginary MEA sidewall of the micro-channel.

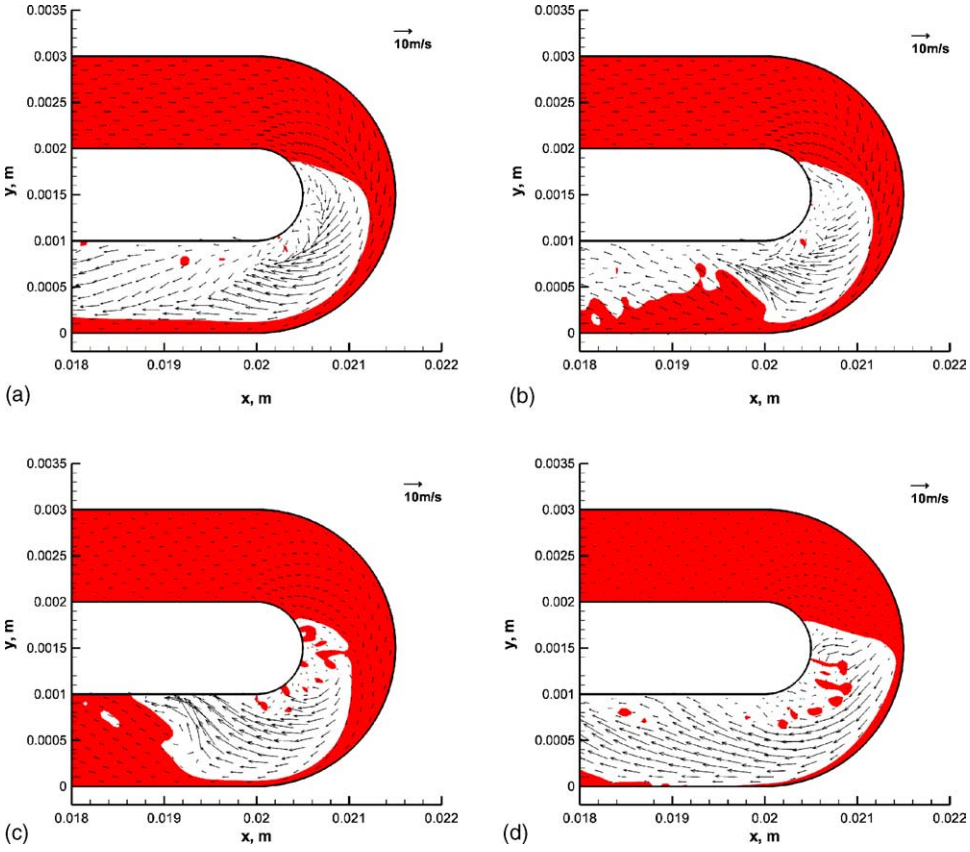

Fig. 17. Water liquid and velocity distribution on the plane near the imaginary MEA sidewall: (a) $t = 0.80$ ms; (b) $t = 1.05$ ms; (c) $t = 3.05$ ms; (d) $t = 4.05$ ms.

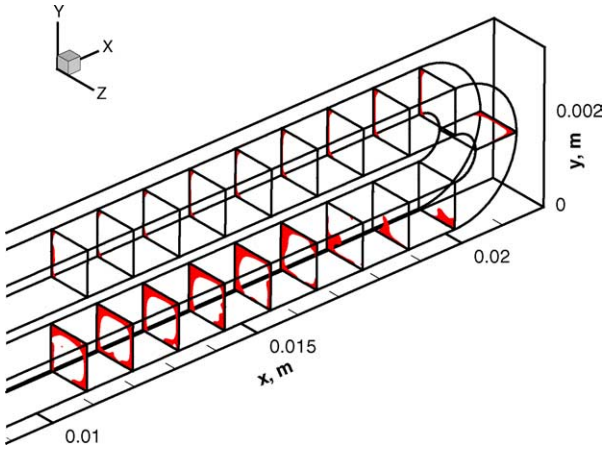

Fig. 18. Water liquid distribution in cross-sections along the main flow direction at $t = 3.75$ ms.

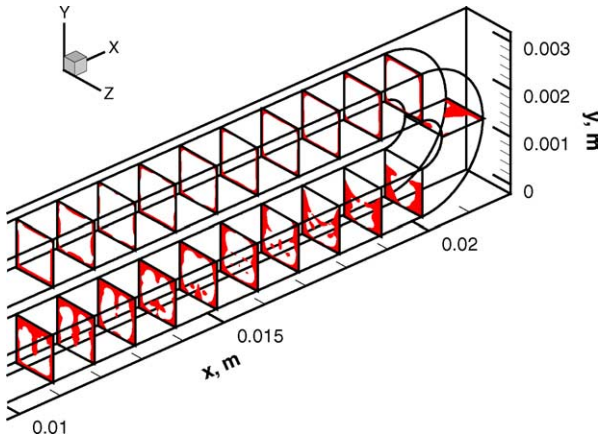

Fig. 20. Water liquid distribution in cross-sections along the main flow direction at $t = 3.0$ ms.

3.5. Case 5: a liquid water film covering all interior surfaces of the micro-channel

The extreme operating condition inside the micro-channel of a PEM fuel cell could be simulated by covering all interior surfaces with a liquid water film (0.1 mm thick). The authors' interest was water behavior on the electrode surface (imaginary MEA sidewall) and the water liquid distribution in the airflow along the micro-channel.

3.5.1. Water behaviors on the electrode surface

Water behavior on the electrode (or MEA) surface is very important for better understanding the transport mechanism inside a channel, fuel cell design and optimization. In this study, the focus was on water distribution on the imaginary MEA sidewall in the lower straight channel (after-bend section).

Similar to Case 4, the formation of a void space in the bend area could be observed. However, in Case 4, once the void space was formed, it continuously expanded towards the exit of the lower channel. In Case 5, however, as long as the water was continuously provided from the upper channel, the position and the shape of the void space remained almost unchanged as shown in Fig. 19. The essential reason for this stable void space is attributed to the increased amount of water. In addition, with more water distributed on the four interior channel surfaces, the interaction (friction) between the airflow and the water liquid became stronger which could lead to significant pressure drop compared to Case 4. Correspondingly, the kinetic energy of the airflow decreased. Therefore, less dragging force could be provided to the water attached to the imaginary MEA sidewall. In other words, the forces acted on the water, namely surface tension, wall adhesion, gravity, and shear force from the airflow, might get balanced, thus forming a stable water pattern on the electrode (or MEA) surface in the lower channel. Without the forward-moving void space as observed in Case 4, most of the electrode (or MEA) surface in the lower channel was covered by liquid water film. This is probably the right operating condition for a working fuel cell. Obviously, the liquid water film could block the reactant (air) entering the reaction sites, thus decreasing the fuel cell performance. From a fuel cell operation of view, it might be helpful if an adjustable air pressure was provided to the airflow in case flooding occurred inside the micro-channel.

3.5.2. Water liquid distribution in the airflow along the main flow direction

Fig. 20 shows the water distribution in cross-sections along the flow direction at $t = 3.0$ ms. It could be observed that, the originally uniformly distributed water film remained attached to the interior channel surfaces; even the bend could not detach the water film from them. This indicates that once the water transport condition inside the channel is depressed (too much water covering the interior surfaces), it would be

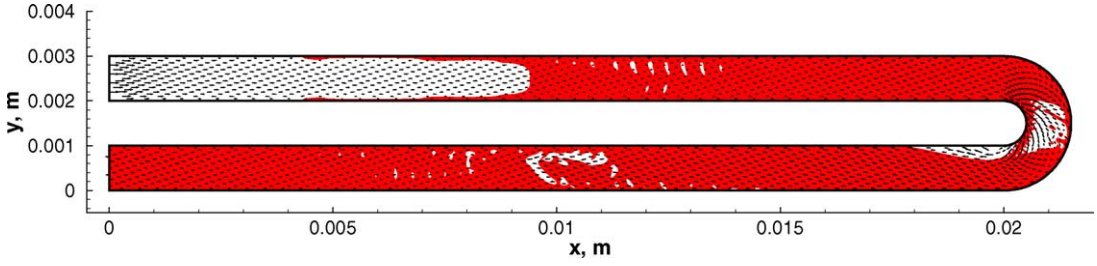

Fig. 19. Water behavior on the plane near the imaginary MEA side wall at $t = 2.55$ ms.

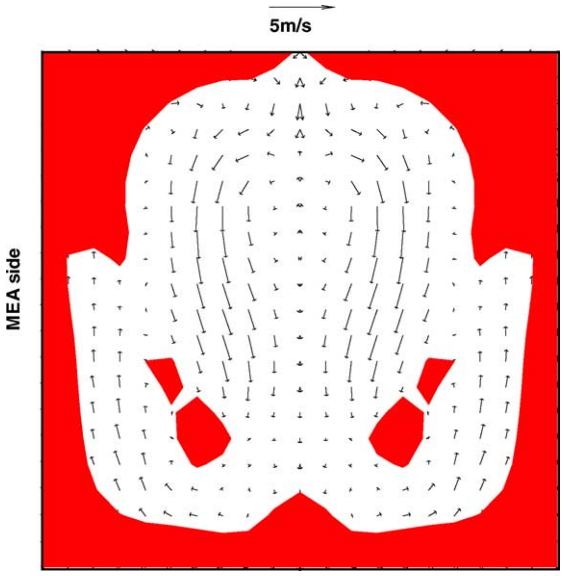

Fig. 21. Water and velocity distribution in cross-section $x = 0.016$ m in lower channel at $t = 2.05$ ms.

very difficult to recover to its healthy condition (less water covering the electrode surface) since no extra forces would be provided to the attaching water liquid to move it away. Fig. 20 also indicates that the gravity effect became significant due to the increased amount of water.

Fig. 21 shows a typical velocity and water distribution in a selected cross-section ($x = 0.016$ m, lower channel) at $t = 2.05$ ms. It could be observed that interior surfaces of the micro-channel were covered by a thick, non-uniform water liquid film, which might result in not only blockage for reactant diffusion to reaction sites, but also a significant increase of pressure drop along the flow direction.

4. Conclusions

(1) The bend area plays an important role in determining water behavior inside a U-shaped micro-channel.
(2) Water behavior inside a U-shaped micro-channel is mainly due to the combined effects of shear stress from airflow, wall adhesion, gravitational force, and surface tension.
(3) The secondary flow induced by the interaction of water liquid and airflow in bend area strongly affects water behavior in the bend and after-bend area. It not only drives water to the surrounding surfaces, but also affects water distribution in the airflow inside the micro-channel.
(4) The void space in bend area may make positive contribution to the removal of liquid water from the electrode surface; however for the case with larger amount of water, the void space effect becomes less significant.
(5) In the case with larger amount of water in the two-phase flow, the simulation results showed that the after-bend water distribution might block the reactant supply to the reaction sites and the reactant transport inside the gas flow channel, thus decreasing the fuel cell performance.

Acknowledgements

The authors are grateful for the support of this work by the Auto21 Networks of Centre of Excellence Grant D07-DFC, the Natural Sciences and Engineering Research Council of Canada (NSERC), and the Graduate School at the University of Windsor.

References

[1] S. Gottesfeld, Adv. Electrochem. Sci. Eng. 5 (1997) 195.
[2] T.E. Springer, T.A. Zawodzinski, S. Gottesfeld, J. Electrochem. Soc. 138 (1991) 2334.
[3] T.V. Nguyen, R.E. White, J. Electrochem. Soc. 140 (1993) 2178.
[4] D.M. Bernardi, M.W. Verbrugge, AIChE J. 37 (1991) 1151.
[5] D.M. Bernardi, M.W. Verbrugge, J. Electrochem. Soc. 139 (1992) 2477.
[6] T.F. Fuller, J. Newman, J. Electrochem. Soc. 140 (1993) 1218.
[7] M.C. Kimble, N.E. Vanderborgh, Proceedings of the 25th Intersociety Energy Conversion Engineering Conference, vol. 3, 1992, p. 413.
[8] J.S. Yi, T.V. Nguyen, J. Electrochem. Soc. 145 (1998) 4.
[9] V. Gurau, H. Liu, S. Kakac, AIChE J. 44 (1998) 2410.
[10] K. Amakawa, N. Uozumi, U.S. Patent No. 4,615,955 (1986).
[11] T.V. Nguyen, J. Electrochem. Soc. 143 (1996) L103.
[12] D.P. Wilkinson, H.H. Voss, K.B. Prater, U.S. Patent No. 5,252,410 (1993).
[13] M.S. Wilson, U.S. Patent No. 5,641,586 (1997).
[14] S. Dutta, S. Shimpalee, J.W. Van Zee, Int. J. Heat Mass Transfer 44 (2001) 2029.
[15] S. Dutta, S. Shimpalee, J.W. Van Zee, J. Appl. Electrochem. 30 (2000) 135.
[16] T. Fukano, A. Kariyasaki, Nucl. Eng. Des. 141 (1993) 59.
[17] M. Fouran, S. Bories, Int. J. Multiphase Flow 21 (1995) 621.
[18] L. Galbiati, P. Andreini, Int. Commun. Heat Mass Transfer 21 (1994) 461.
[19] FLUENT 6.1 User's Guide, FlUENT.
[20] J.U. Brackbill, D.B. Kothe, C. Zemach, J. Comput. Phys. 100 (1992) 335.